Pion production in 5-GeV/c peripheral antiproton-emulsion interactions

B. Bhowmik and S. Singh
Department of Physics and Astrophysics, University of Delhi, Delhi, India
(Received 20 October 1971)

The aim of the present work is to investigate the role of resonances in multiple-pion production in the annihilation and nonannihilation interactions of 5-GeV/c antiprotons with the free or quasifree nucleons of emulsion nuclei. The separation of these interactions has been made on the basis of a plot of median angle against impact parameter for individual events. A phenomenological investigation of the following aspects has been made: the average survival probability, multiplicity, inelasticity, azimuthal and c.m. angular distributions, total and longitudinal momenta in the c.m. system, and transverse momentum and its dependence on multiplicity, c.m. angle, and longitudinal momentum. It has been observed that the features of nonannihilation interactions are similar to those of p-N interactions at comparable primary energies. It has also been inferred that $N^*(1238)$ and $\bar{N}^*(1238)$ are responsible for the production of almost all the pions in nonannihilation events. In the annihilation interactions, dominant production of ρ- and ω-meson resonances has been observed. In the over-all annihilation channels, production of ρ seems to be much larger than that of ω and the former appears to be emitted preferentially in the forward and the latter in the backward direction of the c.m. system.

I. INTRODUCTION

Although $\bar{p}$-p total cross sections are now available up to incident momentum of 50 GeV/c,[1] the characteristics of the mechanism of particle production in these interactions have been studied only up to 9 GeV/c.[2-12] These investigations have revealed that, with increasing momentum of the primary antiproton, the cross sections of nonannihilation channels compete with those of the annihilation ones, and indeed at ~6 GeV/c almost half[10] of the inelastic cross section is attributed to the former process. The effective-mass distributions of various combinations of final-state particles reveal[11] copious production of nucleon and meson resonances in the nonannihilation and annihilation processes, respectively. However, no conclusive attempts have been made so far to understand the behavior of various parameters (e.g., transverse momentum, inelasticity) of created particles in terms of resonance formation. Such an investigation yields several finer details (e.g., frequency, velocity, and direction) of the resonances produced. Attempts in this direction have been made in the present paper.

Although a clear-cut classification of nonannihilation events by the direct identification of the surviving antiproton is not feasible in emulsion experiments, a satisfactory selection of annihilation and nonannihilation events has been made on the basis of a plot of median angle against impact parameter in individual events. The general characteristics of thus classified nonannihilation events have been found to be very similar to those of p-N interactions at comparable primary energies. These events are peripheral in nature and have been found to be dominated by the production of $N^*(1238)$ and $\bar{N}^*(1238)$. The annihilation events, on the other hand, are characterized by low impact parameters and these interactions are essentially statistical in nature. However, the majority of the final-state particles appear to be decay products of slowly moving ρ- and ω-meson resonances—the latter moving preferentially in the backward direction in the c.m. system. These results have been obtained from a detailed study of inelasticity, azimuthal and c.m. angular distributions, transverse momentum (p_t) and its dependence on multiplicity, angle of emission, and longitudinal momentum of the created particles.

II. EXPERIMENTAL DETAILS

A. Exposure

In the present experiment, we have employed 15 plates of a stack consisting of 20 cm×10 cm NIKFI-R emulsion pellicles. The stack was exposed to an antiproton beam of momentum (5 ± 0.025) GeV/c at CERN. The flux of the beam antiprotons was 13 333/cm^2, with a muon contamination of ~3%. The original thicknesses of the pellicles were not recorded. However, in the present experiment, its mean value for each plate was estimated from the range distribution of muons from π-μ-e decay events (Appendix A).

B. Scanning and Selection Criteria

Scanning was carried out by an "along the track following" method starting with 1 cm from the leading edge of the emulsion plate. A total of 527 interactions was obtained by following 136.84 meters of antiproton track length. After correct-

ing for 3% muon contamination of the beam, the mean-free path was found to be 25.2 ± 1.3 cm, which does not seem to be inconsistent with the value (27.6 ± 0.1) cm obtained by Raghvan *et al.*[13] in G5 emulsion, since the density of NIKFI-R emulsion is higher[14] than that of G5. The mean-free path for protons at this incident momentum is about 1.5 times[15] the present value for the antiproton interactions. The lower value in the present case stems from additional annihilation channels.

In order to select the antiproton-nucleon events from the total sample, the following well-known criteria were adopted:

1. The event must have no black and not more than one gray track associated with it. The gray track must be in the forward direction in the laboratory system.
2. There must be no recoil, blob, or low-energy electron associated with the event.

In this manner 111 events were classified as probable antiproton-nucleon interactions. Out of these, the number of events with even and odd number of prongs is 66 and 45, respectively. The former represent the interactions of $\bar{p}$ with free or quasifree protons, whereas the latter are due to the interactions with the bound neutrons of emulsion nuclei. Assuming plausibly that the number of interactions with bound protons and neutrons is equal, we are left with 21 events due to collisions with free protons. In this manner ~80% of the selected events are due to collisions with bound nucleons of emulsion nuclei. Therefore, it appears that in the majority of the events, the multiplicity, angles, and energies of the secondary particles get modified due to the intranuclear interactions. However, the rigid selection criteria adopted permit the selection of only those events in which the target excitation is very small, and hence the chances of intranuclear interactions are negligible.

C. Measurements

Ionization and multiple-Coulomb-scattering measurements were performed on all the secondary shower tracks having dip angles less than 10° in the unprocessed emulsion. On an average, 1500 blobs were counted on each suitable track. The variation of blob density with depth was determined by performing a blob count on the beam tracks. All ionization measurements were normalized to correspond to the blob density in the central region of the pellicles. It is well known[16] that the contribution of spurious scattering to the observed Coulomb signal of a track varies not only with the cell length and depth and region of the emulsion layer, but also from track to track, almost randomly with the nature and energy of the particle. In view of this observation, it seems to be more rational to eliminate the contribution of spurious scattering from the observations on individual tracks, rather than to subtract a constant amount (as has been done previously) of spurious scattering for a given cell length, estimated from observations on beam tracks. Therefore, the relative merits of various methods of noise elimination were tested with observations on beam tracks (Appendix B) and the method giving the most consistent results was applied to obtain the $p\beta$ (momentum times velocity) of the secondary shower tracks.

D. Identification

For the secondary shower tracks, the observed multiple-Coulomb scattering ($p\beta$) has been plotted in Fig. 1 against the blob density (b^*), normalized to that of the beam tracks. The curve given by Nicoletta *et al.*[17] was used for obtaining the g^*-$p\beta$ curves. The g^* was converted into b^* for the present stack by using the well-known[18] relation $b = ge^{-\varepsilon\alpha}$, where g is the grain density of the track

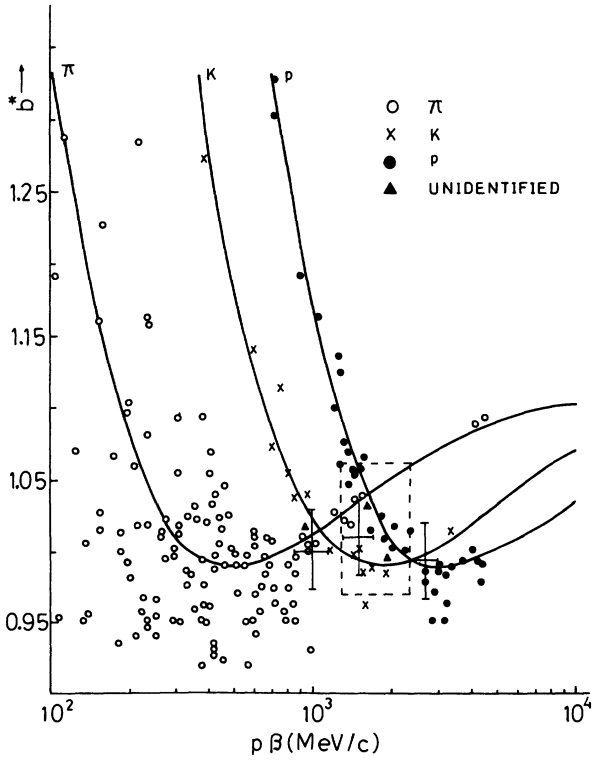

FIG. 1. Plot of normalized blob density (b^*) against $p\beta$ for shower particles. The particles inside the rectangle formed by broken lines have been identified by the η method.

and α is an empirical parameter approximately equal to the mean distance between centers of two crystals, which after development can just be resolved in the microscope. α was determined by the gap-density method of Fowler and Perkins.[18]

The average statistical errors in the values of $p\beta$ and b^* were 10% and 2.8%, respectively, as indicated in the figure. The cell length for scattering measurements was chosen to keep the signal to noise ratio >2 and the statistical error less than 15%. It is clear from Fig. 1 that in the region where the b^*-$p\beta$ curves overlap, the identification is not feasible. Especially in the range of the values of $p\beta$ from 1.3 GeV/c to 2.4 GeV/c, it is difficult to ascertain the identity simply on the basis of b^* and $p\beta$ measurements. To resolve the ambiguity of identity in such cases, we have made use of the additional information on the angle of emission θ and obtained a distribution of $\eta \equiv p_t/\mu = \gamma\beta \sin\theta$ simply from g^* and θ measurements. Here μ, βc, and γ are, respectively, the rest mass, velocity, and Lorentz factor of a shower particle. The distribution of η has been shown in Fig. 2, which clearly suggests that particles having their η values less than 0.3 are most probably[19] of protonic mass, and those having $\eta > 0.7$ are almost exclusively pions. Obviously the particles which have η such that $0.3 < \eta < 0.7$ are most probably kaons. A more complete discussion on identification of shower particles based on their η values is given in Ref. 19. Table I shows the values of η and the corresponding identities, based on above arguments, for the shower particles having $p\beta$ in the range 1.3 GeV/c to 2.4 GeV/c. In Fig. 1, the points corresponding to these particles have been shown enclosed in a rectangular box of broken lines. Thus it is clear that in cases where the conventional (b^*, $p\beta$) method is of no avail, the method based on η distribution can be employed fruitfully, and the identity of shower particles could be established. However, in the present case three of the particles having their (b^*, $p\beta$) points in the overlap region of the curves could not be identified.

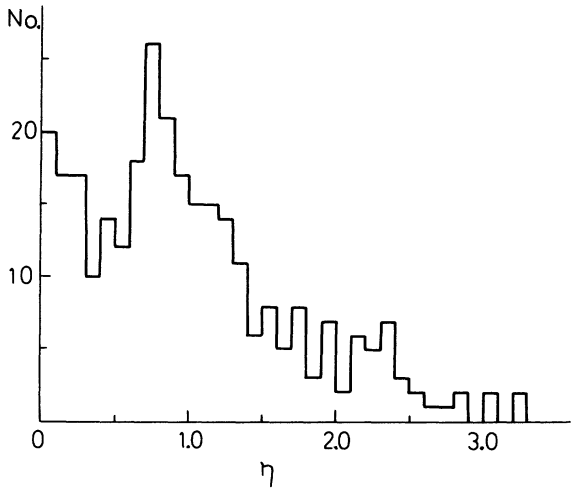

FIG. 2. The η distribution of shower particles produced in $\bar{p}$-N interactions.

As a result of the dip-selection criterion, the tracks having dip angles greater than 10° in the unprocessed emulsion remained unmeasured. To take account of this bias, each track was assigned a geometrical factor depending on its space angle. After applying correction for geometrical factor, it is found that of the total number of identified charged shower particles, the $\pi^{\pm}$, $p/\bar{p}$, and $K^{\pm}$ constitute 80%, 12%, and 8%, respectively.

III. SELECTION OF ANNIHILATION AND NONANNIHILATION EVENTS

In the current literature, inelastic interactions of antiprotons, in which an incident antiproton reemerges or suffers charge exchange to antineutron, along with production of other secondary particles, are generally termed as nonannihilation interactions. In the present experiment, it is not possible to distinguish the surviving antiproton from a secondary proton by direct measurements. Therefore, indirect methods are to be adopted for the identification of annihilation and nonannihilation events. For this purpose, we have studied the distributions of (i) the median angle θ_{med}, i.e., the angle containing half of the shower particles in an event, and (ii) the impact parameter r of the collision of the incident antiproton with a nucleon. Since we are interested in seeing only the trend of variation of θ_{med} with r, it is not essential to have a precise estimation of the impact parameter, which is rather involved. For the present purpose, the impact parameter for each event was calculated by the approximate formula given by Ezawa[20]:

TABLE I. The identities of shower particles in the overlapping region as inferred from their η values.

$p\beta$ (GeV/c)	η	Identity	$p\beta$ (GeV/c)	η	Identity
1.31	1.11	π	1.60	0.70	unidentified
1.33	0.09	$p/\bar{p}$	1.65	0.20	$p/\bar{p}$
1.37	1.78	π	1.65	0.39	K
1.38	0.90	π	1.80	0.07	$p/\bar{p}$
1.40	0.01	$p/\bar{p}$	1.85	0.12	$p/\bar{p}$
1.41	0.51	K	1.90	0.65	K
1.42	0.04	$p/\bar{p}$	1.92	0.30	unidentified
1.48	3.07	π	2.01	0.25	$p/\bar{p}$
1.51	0.06	$p/\bar{p}$	2.05	0.05	$p/\bar{p}$
1.52	0.55	K	2.25	0.17	$p/\bar{p}$
1.55	0.41	K	2.40	0.21	$p/\bar{p}$

$$r = \sqrt{3}\, m \hbar n_s^{1/2}/4Mc\gamma_c ,$$

where n_s is the number of shower particles in an event, $\hbar$ is the Planck constant divided by 2π, and M, c, and γ_c are, respectively, the nucleon mass, velocity of light, and Lorentz factor of the c.m. system of the colliding particles. m is the "sharpness" parameter of the angular distribution of shower particles in the c.m. system, and its estimate is given by[21]

$$m = 2\langle \csc\bar{\theta}\rangle^2/\pi ,$$

where $\bar{\theta}$ is the angle in the c.m. system corresponding to a laboratory angle of emission θ.

The plot of median angle against the impact parameter for all the $\bar{p}$-N events has been shown in Fig. 3. The figure also shows the individual distributions for the median angle and the impact parameter. It is evident from these figures that the sample of $\bar{p}$-N events could be grouped into two classes, namely, those having smaller r and larger θ_{med} and the others which have larger r and smaller θ_{med}. Evidently the former will be rich in annihilation, and the latter in nonannihilation events.[22]

In view of Fig. 3, we have adopted the following criteria for selecting nonannihilation interactions: (i) The median angle must be less than 17.5°; (ii) the impact parameter must be more than 12 units. It was observed that the events in which the leading particle was identified as $p/\bar{p}$ invariably satisfied both these criteria, giving further confidence in the method of classification. In this way, we have formed a sample of 52 events enriched in annihilation interactions and of 59 events consisting chiefly of the nonannihilation ones. It indicates that the cross sections for annihilation and nonannihilation channels in 5 GeV/c $\bar{p}$-N interactions are nearly equal, a conclusion in agreement with the observations of Böckmann *et al.*[10] for hydrogen bubble-chamber (H.B.C.) data at 5.7 GeV/c.

IV. RESULTS

A. The Average Survival Probability

In $\bar{p}$-N interactions, the survival probability is defined as the probability of the primary antiproton emerging as an antiproton after the collision with a nucleon. In the present experiment it is not possible to distinguish a secondary proton from a surviving antiproton. Therefore, we employ indirect means to estimate the number of surviving antiprotons. Since the surviving $\bar{p}$ retains a large fraction of primary energy, it is likely to be projected in the forward direction in the c.m. system; therefore, we assume that all the identified shower particles of protonic mass proceeding along extreme forward direction (<10°) in the c.m. system are antiprotons surviving the collision. In this way the actual number of identified antiprotons is found to be 31 and the number corrected for geometrical losses is 33. The total number of events considered is 111 and the total number of shower particles observed in these events is 338, whereas the corrected number of identified shower

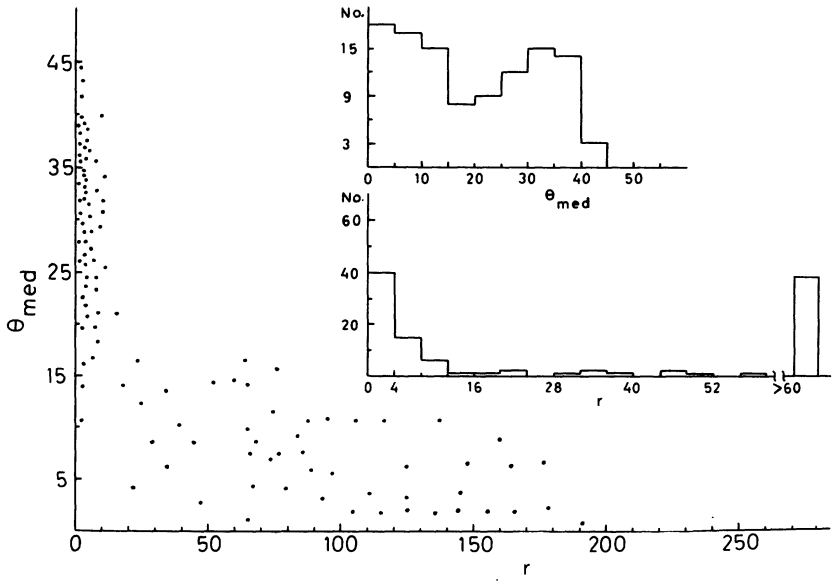

FIG. 3. Plot of median angle (θ_{med}) in degrees, against impact parameter (r) in units of $\sqrt{3}\,\hbar/4Mc\gamma_c$. Insets show separate distributions of θ_{med} and r in the same units.

particles is 349. These data yield the number $N_{\bar{p}}$ of reemergent antiprotons per event as

$$N_{\bar{p}} = (33/349)\times(338/111)$$
$$= 0.29 \pm 0.06 .$$

At 6.1 GeV/c, the value of charge-retention probability for incident proton in p-N interactions was found to be (0.48 ± 0.05) by Daniel *et al.*[23]. The low value obtained in the present case indicates a significant role of annihilation and charge-exchange processes in the $\bar{p}$ interactions.

B. Multiplicity

The over-all mean multiplicity $\langle n_s \rangle$ of shower particles is 3.2 ± 0.3. Its value for the annihilation and nonannihilation events is found to be 4.1 ± 0.5 and 2.1 ± 0.3, respectively. The mean number of pions $\langle n_{\pi^\pm} \rangle$ is obtained as 2.7 ± 0.3, which for annihilation and nonannihilation events is found to be 4.0 ± 0.6 and 1.4 ± 0.2, respectively. The low value in the latter case may be attributed to the fact that the available energy in the c.m. system for the creation of secondary particles is much less than that in the former one.

The values of $\langle n_s \rangle$ and $\langle n_{\pi^\pm} \rangle$ for shower particles produced in the p-N and $\bar{p}$-N interactions at similar primary energies are compared in Table II. It is evident that the results obtained in the present experiment are consistent with those obtained in the hydrogen bubble-chamber experiments.[10] Moreover, the mean values for nonannihilation events exhibit very good agreement with those obtained in the p-N interactions.

The distributions of shower multiplicity for the $\bar{p}$-N interactions and separately for the annihilation and nonannihilation events have been displayed in Figs. 4(a) and 4(b), respectively. The distribution of even n_s has been compared with the hydrogen bubble-chamber data[10] at 5.7 GeV/c. The two distributions are found to be similar. Moreover, the differential distribution of n_s is represented very well by a Poisson distribution, Fig. 4(a), as predicted by the multi-Regge model.[24]

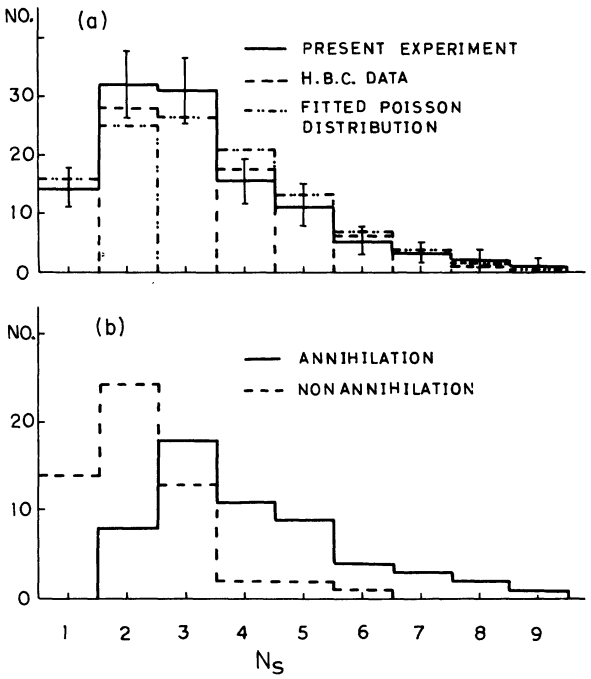

FIG. 4. (a) Distribution of shower multiplicity for all $\bar{p}$-N interactions and its comparison with hydrogen bubble-chamber data and Poisson distribution. (b) Comparison of distributions of shower multiplicities for annihilation and nonannihilation events.

In the multiplicity distributions, an interesting feature has been observed,[25] namely, that the plot of the logarithm of the number of events having shower multiplicity $\geq n_s$ against n_s^2 is approximately a straight line. It has been found to hold well for all types of collisions and at almost all the primary energies. In the present experiment also, this feature is quite evident as displayed in Fig. 5. The agreement of the present results on multiplicity with those from the hydrogen bubble-chamber experiment clearly indicates that there is no significant modification of multiplicity due to probable

TABLE II. Comparison of mean number of particles in $\bar{p}$-N and p-N collisions.[a]

Interaction and beam momentum (GeV/c)	$\langle n_s \rangle$ Over-all	$\langle n_s \rangle$ A	$\langle n_s \rangle$ NA	$\langle n_{\pi^\pm} \rangle$ Over-all	$\langle n_{\pi^\pm} \rangle$ A	$\langle n_{\pi^\pm} \rangle$ NA	Reference
$\bar{p}$-N(5.0)	3.1 ± 0.3	4.1 ± 0.5	2.1 ± 0.3	2.7 ± 0.3	4.0 ± 0.6	1.4 ± 0.2	Present work
$\bar{p}$-p(5.7)	3.8 ± 0.4	...	...	3.1 ± 0.2	4.2 ± 0.4	1.9 ± 0.2	10[b]
p-N(6.1)	...	...	2.2 ± 0.2	...	...	1.6 ± 0.2	23
p-p(4.0)	...	...	...	...	...	1.3 ± 0.3	24

[a] A and NA are symbols for annihilation and nonannihilation, respectively.
[b] These results were calculated from cross sections given for various channels.

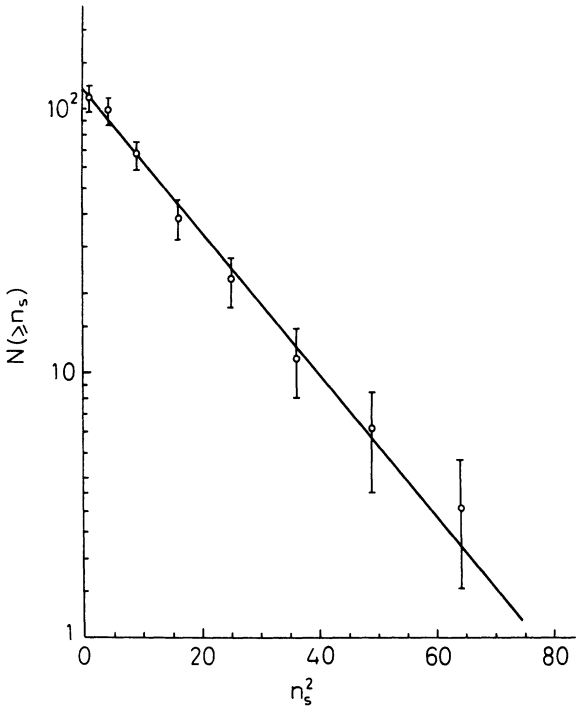

FIG. 5. Plot of number of events (on log scale) having shower multiplicity $\geq n_s$ against n_s^2.

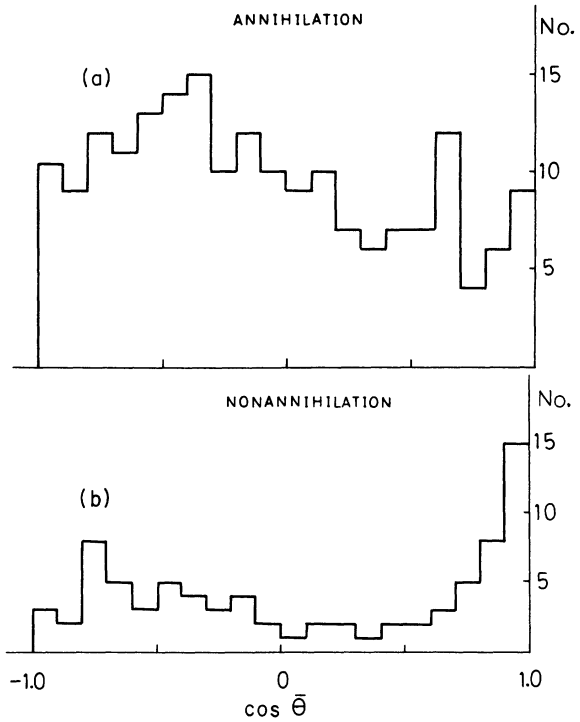

FIG. 6. Angular distributions of charged pions in the c.m. system.

intranuclear interactions in the $\bar{p}$–bound-nucleon interactions.

C. The Angular Distribution of Pions in the c.m. System

The angular distribution of pions created in the nonannihilation interactions has been shown in Fig. 6(b). The distribution shows a clear tendency for fore-aft peaking. However, the forward to backward ratio is found to be 1.02 ± 0.22. The angular distribution of pions produced in annihilation events has been displayed in Fig. 6(a). The forward to backward ratio is (0.65 ± 0.09), which clearly indicates an excess of pions in the backward direction. Such an excess has been seen by earlier authors[4,11] also.

D. The Azimuthal Angular Distribution

The azimuthal angle ϕ of a particle emitted at a space angle θ is given by

$$\sin\phi = \sin\delta \csc\theta ,$$

where δ is the dip angle of the track of the particle. The azimuthal angular distribution may yield useful information on the process of particle production. It was pointed out by Koba and Takagi[26] and Kraushaar and Marks[27] that in the models of high-energy interactions, making an hypothesis of a metastable state in the reaction, one could expect an azimuthal asymmetry for the secondary particles.

The distributions of ϕ for the charged pions produced in the annihilation and nonannihilation events have been displayed separately in Figs. 7(a) and 7(b), respectively. The hypothesis for isotropic emission for the two distributions has been tested on the basis of a χ^2 test. The values of χ^2 have been found to be 2.8 and 11.6, respectively, with 7 degrees of freedom. The expected value of χ^2 at 90% level of confidence is 2.83, which indicates that the azimuthal angular distribution for annihilation events is consistent with isotropy, and that for the nonannihilation ones it shows clearly a tendency for preferred emission.

E. The Momentum Distribution of Pions in the c.m. System

Figures 8 and 9 display the momentum distributions of pions produced in the annihilation and nonannihilation interactions, respectively. The mean values of momenta for the two classes of events are found to be 336 ± 41 and 248 ± 34 MeV/c, respectively. The distribution for the former class shows two humps, suggesting contributions perhaps from two sources.

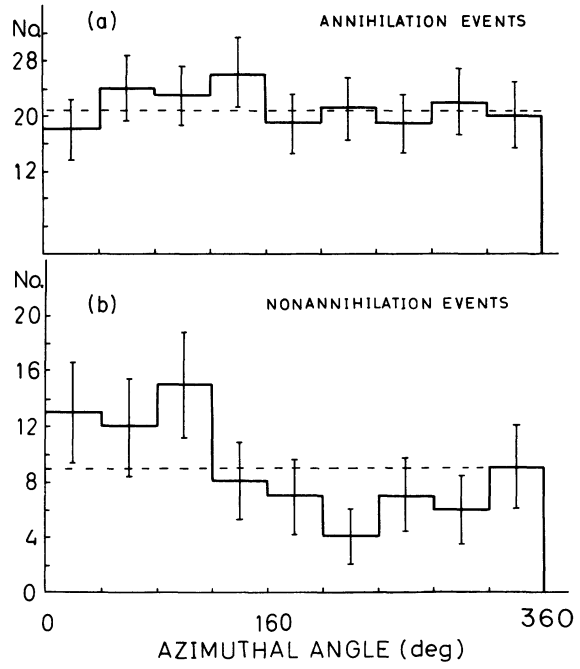

FIG. 7. Azimuthal angular distributions of charged pions. Expected form for isotropic emission is indicated by dashed line.

F. Transverse-Momentum Distribution of Pions

The p_t distributions of pions produced in annihilation and nonannihilation events have been shown in Fig. 10 separately. The average values of p_t for the two distributions are significantly different, and are found to be (236 ± 11) and (173 ± 16) MeV/c, respectively.

In order to obtain the analytical forms of the p_t distributions, we have plotted the fraction F of pions, on log scale, having their transverse momenta $\geq p_t$, against p_t^2 in Fig. 11. It is observed that the experimental points for the case of nonannihilation events are fitted by two straight lines A and B. In case of annihilation events, all the points, except the last two (which have little statistical weight) can be fitted by a single straight line. Consequently the differential p_t distributions are fitted very well by the following distributions:

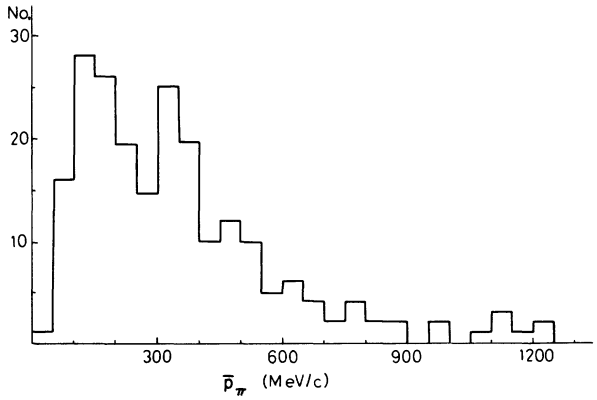

FIG. 8. Distribution of momentum of pions in the c.m. system for annihilation events.

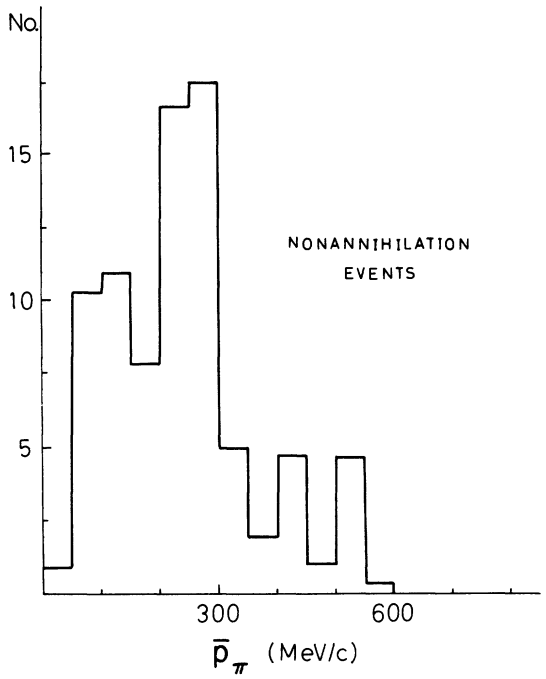

FIG. 9. Distribution of momentum of pions in the c.m. system for nonannihilation events.

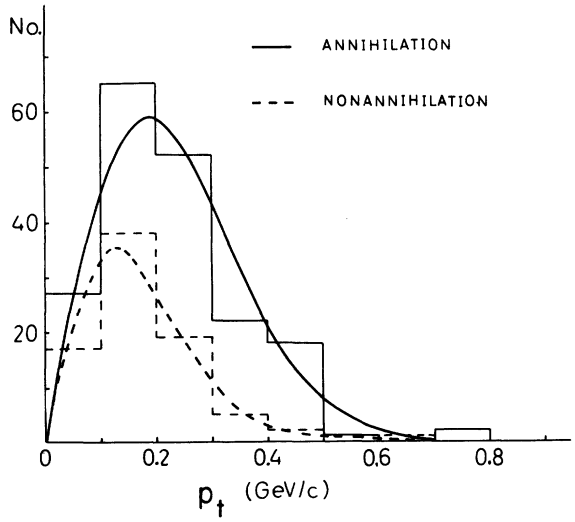

FIG. 10. The transverse-momentum distributions of charged pions produced in annihilation and nonannihilation interactions. The curves show the best-fit distributions (see text).

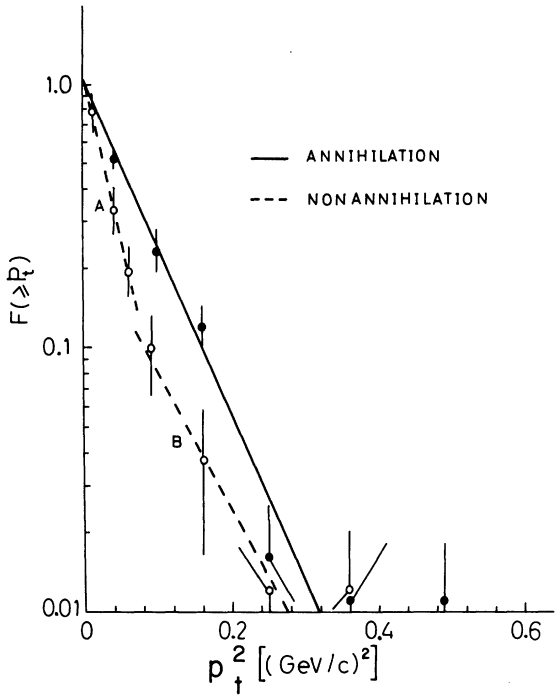

FIG. 11. Plot of fraction (on log scale) of charged pions having transverse momentum $\geq p_t$ against p_t^2.

$$N dp_t = 514 p_t e^{-13.85 p_t^2} dp_t$$

for annihilation events and

$$N dp_t = 415 p_t (e^{-34.40 p_t^2} + 0.13 e^{-12.50 p_t^2}) dp_t$$

for nonannihilation events; here p_t is in GeV/c. The fitted curves in Fig. 10 display these distributions. Thus the p_t distribution of pions from annihilation events follows a Boltzmann form, rather than the shape expected from the Cocconi, Koestler, and Perkins[28] formula. The form of the p_t distribution for nonannihilation events is a two-component Boltzmann distribution of distinctly different parameters. It is similar to that obtained by Friedländer[29] by using the world data on p_t of pions in N-N collisions.

G. Longitudinal-Momentum Distribution of Pions

The distributions, normalized to equal numbers, of the c.m. longitudinal momentum ($\bar{p}_l$) of pions produced in annihilation and nonannihilation events have been shown separately in Fig. 12(a). The distribution for annihilation events seems to be steeper in the backward direction, whereas that for the nonannihilation ones is almost symmetric. The integral plots [$\log F(\geq \bar{p}_l)$ vs $\bar{p}_l{}^2$ as shown in Fig. 12(b)] for both types of events are identical and can be represented very well by two straight lines having different slopes.

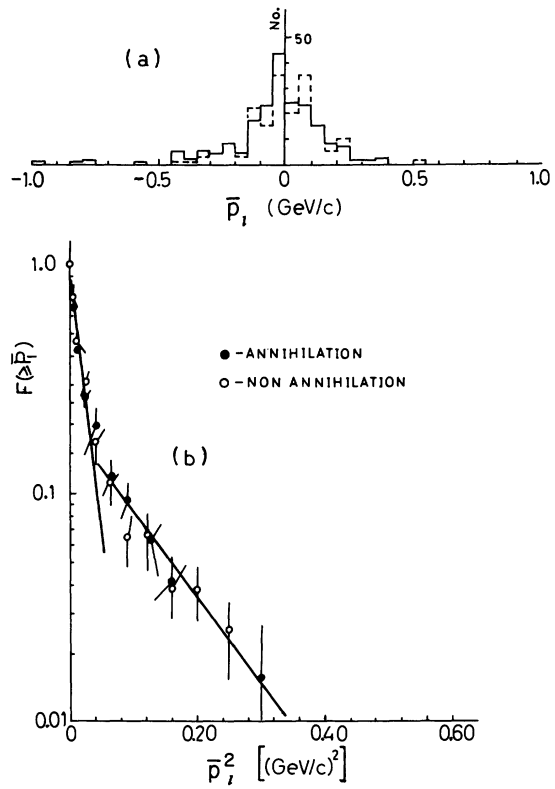

FIG. 12. (a) Distributions of the c.m. longitudinal momentum ($\bar{p}_l$) of charged pions. Solid and dashed lines indicate annihilation and nonannihilation events separately. (b) Plot of fraction of charged pions having their c.m. longitudinal momenta $\geq \bar{p}_l$, i.e., $F(\geq \bar{p}_l)$, on log scale, against $(\bar{p}_l)^2$.

H. Inelasticity

The pion inelasticities K_{NA} and K_A for the nonannihilation and annihilation events, respectively, are defined by

$$K_{NA} = 1.5 \langle n_{\pi^\pm} \rangle_{NA} \langle \bar{E}_\pi \rangle_{NA} / 2M(\gamma_c - 1)$$

and

$$K_A = 1.5 \langle n_{\pi^\pm} \rangle_A \langle \bar{E}_\pi \rangle_A / 2M\gamma_c ,$$

where $\langle n_{\pi^\pm} \rangle$ and $\langle \bar{E}_\pi \rangle$ are, respectively, the average number of charged pions and their mean energy in the c.m. system. The factor 1.5 is due to the assumption that the mean number of neutral pions is half that of the charged ones, an assumption which is valid for pionization process; its possible deviation due to resonance production is discussed in Sec. V.

Substituting the values, we get K_{NA} and K_A as 0.41 ± 0.07 and 0.68 ± 0.12, respectively. The value of K_{NA} agrees very well with 0.45 ± 0.03 as given by Raghavan *et al.*[13] for 5-GeV/c p-N collisions and with 0.44 ± 0.03 obtained by Daniel *et al.*[23] for 6.2-

GeV p-N interactions. It further supports the resemblance between the nonannihilation and p-N interactions.

V. INTERPRETATION OF RESULTS

The azimuthal angular distribution for nonannihilation events is anisotropic. It indicates the presence of nonzero-spin metastable states[26] in the reaction. This merely reaffirms the bubble-chamber observation that in such interactions the nucleon isobars (and/or anti-isobars) are copiously produced.[11] The c.m. angular distribution Fig. 6(b) clearly shows two jets of pions ejected in the forward and backward hemispheres. It obviously suggests that there are two sources of pions moving in opposite directions. These are presumably a pair of an isobar N^* and an anti-isobar $\bar{N}^*$. In a $\bar{p}$-N collision, it is reasonable to assume that the incident $\bar{p}$ gives rise to $\bar{N}^*$, which moves in the direction (forward) of $\bar{p}$ in the c.m. system, and the target nucleon produces N^* which, therefore, moves in the backward direction. For the sake of convenience, we further assume that the N^* ($\bar{N}^*$) moves along the collision axis in the c.m. system.

For the identity of the isobar (and anti-isobar) a clue is offered by the mean value $\langle p_t \rangle$ of the secondary pions. If we assume that N^* ($\bar{N}^*$) decays isotropically in its rest system, then $\langle p_t \rangle$ for its decay pion is given by

$$\langle p_t \rangle = 3.14\,[(M^{*2} - M^2 + M_\pi{}^2)^2 - 4M_\pi{}^2 M^{*2}]^{1/2}/8M^*,$$

where M^*, M, and M_π are the rest masses of the isobar, decay nucleon, and pion, respectively. Thus $\langle p_t \rangle$ is a function of the mass of the parent isobar. The $\langle p_t \rangle$ for the pions from the decay of $N^*(1238)$ [$\bar{N}^*(1238)$] is found to be 172 MeV/c, which coincides with the observed value of (173 ± 16) MeV/c. Higher isobars undergoing similar decays will yield too-high values for $\langle p_t \rangle$. Therefore, their consideration is disregarded. For a given mass of the isobar, the mean value of the longitudinal momentum of pions in the c.m. system, i.e. $\langle \bar{p}_l \rangle$, depends on the velocity of the parent isobar. From this consideration the mean velocity of the isobar in the c.m. system has been estimated to be about $0.6c$.

Thus for the nonannihilation interactions, we make the hypothesis that all the pions are the decay products of $\bar{N}^*(1238)$ and $N^*(1238)$ which move along the collision axis with velocities $0.6c$ and $-0.6c$, respectively, in the c.m. system. Furthermore, from the observed F/B ratio ~1.0, we conclude that the frequencies of the isobar and anti-isobar in the over-all nonannihilation channels are equal. We shall analyze the consequences of this hypothesis.

We now extend similar arguments for the case of annihilation interactions. The azimuthal angular distribution of pions is found to be isotropic. This does not necessarily mean the absence of metastable states in the reaction because the sample of pions comes from a "composite" event consisting of many individual annihilation events. If in individual events the directions of emission of metastable states or resonances are randomly distributed, then obviously the anisotropy will be masked in the composite distribution. Moreover, if the resonances are spinless (i.e., meson resonances) and are produced statistically, anisotropy may not at all be detected in such an azimuthal distribution.[27] If the process of annihilation were purely statistical without involving resonant states in the reaction, we would have obtained an isotropic angular distribution of pions in the c.m. system; but the angular distribution shows clear excess of pions in the backward direction. Thus it is evident that annihilation, instead of resulting in simple pionization governed by statistical mechanism, is dominated by the formation of resonances.

The identity of the associated resonance can be inferred from the observed value of $\langle p_t \rangle$ of pions, which is 236 ± 11 MeV/c. The meson resonances which involve charged pions in their most prominent decay modes and which impart to their decay pions $\langle p_t \rangle$ round about the observed value are ρ and ω. The most prominent decay modes of ρ and ω are $\rho \to 2\pi$ and $\omega \to 3\pi$, and the $\langle p_t \rangle$ for their decay pions in their rest systems are 273 and 172 MeV/c, respectively. If we assume that all the observed pions are simply the decay products of only[11] the ρ and ω then the observed value of $\langle p_t \rangle$ requires the frequencies of ρ and ω to be 65% and 35%, respectively. The preferential directions of emission of ρ and ω in the c.m. system are indicated by the c.m. angular distribution of charged pions. This distribution shows a significant excess of charged pions in the backward direction. On the other hand, ω produces more charged pions than the ρ, therefore, it seems plausible to assume that ω is emitted preferentially in the backward direction and hence the ρ moves in the forward direction of the c.m. system. For simplicity, we further assume that ρ and ω move along the collision axis. As these resonances have almost equal masses and are produced in a basically statistical process, both of them should have, on an average, equal velocities. The mean value of the c.m. longitudinal momentum of pions, as in the case of the nonannihilation events, suggests that the average velocity of ρ and ω should be ~$0.4c$.

Thus for the annihilation events, we make the hypothesis that the observed pions are dominantly the decay products of ρ and ω which move, on an average, with velocities $0.4c$ and $-0.4c$, respectively, along the collision axis in the c.m. system, and their frequencies of production are 65% and 35%, respectively.

We shall discuss some of the observations on angular distribution, inelasticity, and transverse momentum of pions in the light of above hypotheses for the annihilation and nonannihilation processes.

Let us consider the momentum dependence of the forward to backward ratio (F/B) as displayed in Table III. Although the statistical errors are large, the general trends for the two types of interactions are apparently quite different. The nonannihilation events show practically the same F/B ratio (~1.0) for the whole momentum range, whereas the annihilation events display some momentum-dependent asymmetry. In view of equal frequencies and velocities of $N^*(1238)$ and $\bar{N}^*(1238)$, we see that they decay into an equal number of charged pions in the forward and backward directions irrespective of the momentum of pions. On the other hand, in the annihilation events the ρ- and ω-meson resonances decay most frequently into one and two charged pions, respectively. Their decay pions have different average momenta. Thus in annihilation events, the presence of a momentum-dependent asymmetry of charged pions is not inconsistent with the hypothesis.

On the assumption that neutral to charged pion ratio is 0.5, the pion inelasticity K_A for annihilation events was found to be 0.68 ± 0.12. However, considering the above hypothesis, this ratio could be greater than 0.5. In almost 100% of the cases ρ decays as $\rho^{\pm} \to \pi^{\pm}\pi^0$, and in 90% of the cases ω decays as $\omega \to \pi^+\pi^-\pi^0$ and in about 9% of the cases as $\omega \to \pi^0\gamma$. Thus if we take the weighted average of these processes with the above-mentioned production frequencies of ρ and ω, we obtain

$$\langle n_{\pi^0} \rangle / \langle n_{\pi^{\pm}} \rangle \simeq 0.8$$

instead of 0.5 as assumed in Sec. IV H. Using this value one obtains $\langle n_{\pi^{\pm}} \rangle + \langle n_{\pi^0} \rangle = (7.2 \pm 1.1)$, which is in excellent agreement with (7.3 ± 0.6) as obtained by Böckmann *et al.*[10] for 5.7-GeV/c $\bar{p}$-p annihilations. [This agreement also leads to the conclusion that $\langle p_t \rangle$ (and hence the energies and angles of the secondary particles) and $\langle n_{\pi^{\pm}} \rangle$ have not been significantly affected by the probable intranuclear interactions in the $\bar{p}$-N (bound) collisions.] Then the value of K_A becomes (0.82 ± 0.14), which indicates that almost the whole energy is consumed in the creation of pions. On the other hand, the low value of inelasticity $K_{NA} = (0.41 \pm 0.07)$ can be understood well in the resonance model for the nonannihilation interactions. In the decay process $N^*(\bar{N}^*) \to N(\bar{N})\pi$, an isobar of mass M^* transfers an energy equal to $(M^{*2} - M^2 + M_\pi^2)/2M^*$ to its decay pion in its rest system. Thus a pion from the decay of $N^*(1238)$ $[\bar{N}^*(1238)]$ will carry only about 20% of the primary energy in the resonance rest system. In the c.m. system, a pion produced according to the above mentioned hypothesis will have energy, on an average, equal to 339 MeV, which does not seem to be inconsistent with the observed value of $\langle E_\pi \rangle = (297 \pm 32)$ MeV. Thus the hypothesis accounts for the observed value of inelasticity reasonably well.

It is interesting to study the variation of $\langle p_t \rangle$ with multiplicity n_s. Table IV shows the relevant data. The mean values of p_t (denoted as $\langle p_t \rangle'$) have been calculated for composite events of different multiplicities. Since the number of pions in each multiplicity subgroup is not equal, we have calculated the relative percentage contribution (R) of each subgroup to the over-all $\langle p_t \rangle$. If G_{ij} is the geometrical factor of ith pion in the jth multiplicity subgroup, we define the percentage relative contribution R of the jth multiplicity subgroup to the over-all p_t as

$$R_j = 100\left(\langle p_t \rangle_j' \sum_i G_{ij}\right) \Big/ \left(\langle p_t \rangle \sum_i \sum_j G_{ij}\right) .$$

Thus R_j may be treated as the normalized value of the mean transverse momentum for the jth multi-

TABLE III. The forward to backward (F/B) ratio of pions as a function of their momentum in the c.m. system.

Momentum MeV/c	F/B Annihilation	F/B Nonannihilation
<200	0.56 ± 0.15	1.14 ± 0.42
200–400	0.85 ± 0.19	0.86 ± 0.26
>400	0.53 ± 0.13	0.87 ± 0.49

TABLE IV. Mean value of p_t of pions for different multiplicities.

Type of interaction	n_s	$\langle p_t \rangle'$ (MeV/c)	Relative contribution R (%)	Over-all $\langle p_t \rangle$ (MeV/c)
Annihilation	2–3	193 ± 29	16	236 ± 11
	4–5	198 ± 21	44	
	≥6	295 ± 41	40	
Nonannihilation	1–2	164 ± 20	48	173 ± 16
	≥3	181 ± 31	52	

plicity subgroup.

The values of R indicate that for annihilation events the mean value of transverse momentum is multiplicity-dependent and the relative contribution to over-all $\langle p_t \rangle$ for $n_s \geq 4$ is almost constant, but it is significantly greater than that for $n_s \leq 3$ events. Thus in low-multiplicity events, if any of the ρ and ω resonances are produced at all, it could only be ω which imparts generally low values of p_t to its decay pions. In hydrogen bubble-chamber experiments, most of the authors[11] have not detected the presence of any intermediate resonant states in low-multiplicity channels such as $\bar{p}p \to \pi\pi$. On the other hand, the production of ρ becomes increasingly dominant as one goes to high-multiplicity annihilation channels. Since the decay pions from ρ have a larger mean value of p_t than that of the decay pions from ω, the mean p_t for higher multiplicities is expected to be larger. This is evident from Table IV.

In the case of nonannihilation interactions, the values of p_t are independent of multiplicity, and the contribution from both the low- and high-multiplicity events to the over-all $\langle p_t \rangle$ is almost equal. This implies that for all the multiplicities, the production of isobars and anti-isobars is equally dominant.

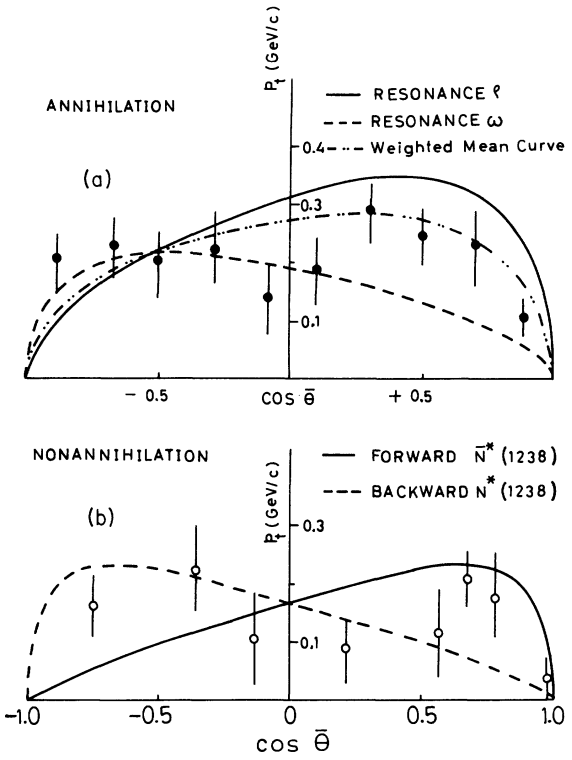

FIG. 13. Variation of transverse momentum (p_t) of charged pions with $\cos\bar{\theta}$. The curves correspond to the decay pions of (a) ρ and ω moving with velocities $0.4c$ and $-0.4c$, respectively, along the collision axis in the c.m. system. (b) $\bar{N}^*(1238)$ and $N^*(1238)$ moving with velocities of $0.6c$ and $-0.6c$, respectively, along the collision axis in the c.m. system.

The trends of variation of p_t with emission angle and longitudinal momentum ($\bar{p}_l$) in the c.m. system can be accounted for well on the two hypotheses mentioned above. Figure 13 shows the plot of the mean values of p_t of identified pions against $\cos\bar{\theta}$, where $\bar{\theta}$ is the pion emission angle in the c.m. system. The p_t of pions in annihilation events shows small variation, whereas the same undergoes comparatively larger fluctuations in nonannihilation events. In Fig. 13 the curves have been drawn for the pions from the decays of the meson resonances. The velocities and directions of emission used in the calculations were the same as mentioned in the hypothesis. Although the statistical errors are large, the experimental points clearly follow the trend depicted by the calculated curves. In case of annihilation events, the weighted mean curve has been calculated assuming the frequencies of ρ and ω resonances in the ratio 2 : 1. This curve seems to pass through the majority of experimental points.

The plots of $\langle p_t \rangle$ against $\langle \bar{p}_l \rangle$ have been shown in Figs. 14(a) and 14(b) for the nonannihilation and annihilation events, respectively. The curves have been obtained on the above hypotheses. Obviously most of the experimental points lie within the calculated curves and the general trends are well described by the curves for both the types of events.

VI. DISCUSSION AND CONCLUSIONS

The good agreement of our results with the hydrogen bubble-chamber data on mean multiplicity, neutral- to charged-pion ratio, and cross section for annihilation and nonannihilation events suggests that (a) the modification in the multiplicity, energies, and angles of the secondary particles due to probable intranuclear interactions in the $\bar{p}$-N (bound) collisions is negligible and (b) our method of separating annihilation and nonannihilation events is quite valid. The elimination of spurious scattering by the statistical method has resulted in a more reliable estimation of the momentum of secondary shower particles. The identification of most of the shower particles even in the overlap region of the b^*-$p\beta$ plot by a new method based on their η values has substantially reduced the number of unidentified shower particles.

The observed asymmetry of azimuthal angular distribution of pions indicates the presence of intermediate resonant states in these reactions. The observation of fore-aft peaking in the c.m. angular distribution of pions suggests that the pions originate effectively from two sources mov-

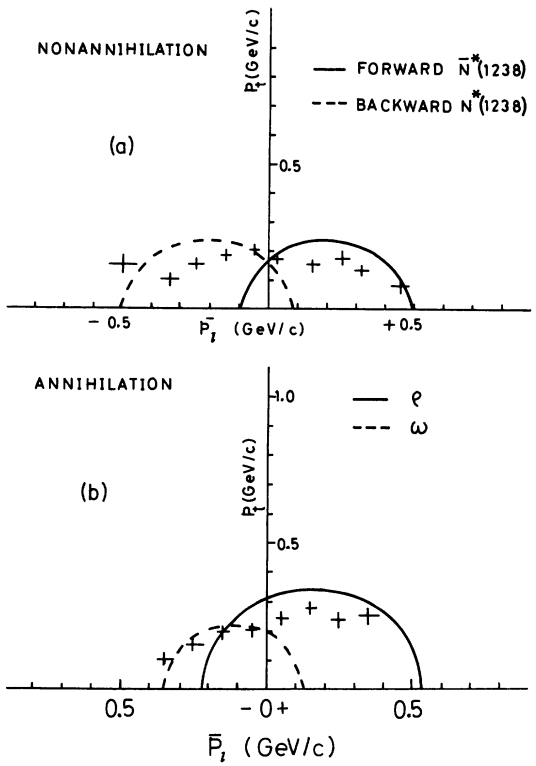

FIG. 14. Plot of transverse momentum (p_t) against the longitudinal momentum ($\bar{p}_l$) in the c.m. system. The curves correspond to the decay pions of (a) $\bar{N}^*(1238)$ and $N^*(1238)$ moving with velocities of $0.6c$ and $-0.6c$, respectively, along the collision axis in the c.m. system, (b) ρ and ω moving with velocities $0.4c$ and $-0.4c$, respectively, along the collision axis in the c.m. system.

ing in opposite directions in the c.m. system. These sources are presumably the $\bar{N}^*(1238)$ and $N^*(1238)$, as suggested by the magnitude of mean transverse momentum $\langle p_t \rangle$ of created pions. The F/B ratio of charged pions in the c.m. system is ~1, which indicates almost equal frequencies of the isobar and anti-isobar. The observed trend of variation of p_t of pions with their longitudinal momentum ($\bar{p}_l$) reveals that the anti-isobar and isobar move, on an average, with velocities of $0.6c$ and $-0.6c$, respectively, almost along the collision axis in the c.m. system. The annihilation events are understood in terms of central collisions and are explained well on the basis of dominant production of ρ and ω resonances. The mean values of p_t and energy of pions in the c.m. system suggest that the production of ρ should be much more predominant than that of ω. The p_t-$\bar{p}_l$ distribution of pions suggests that the average velocities of each of ρ and ω is $0.4c$ in the c.m. system, and the excess of charged pions in the backward direction indicates that ω is emitted preferentially in the backward, and ρ in the forward direction. This assumption of preferential emission explains well also the variation of p_t with c.m. angle of emission.

ACKNOWLEDGMENTS

We are grateful to Professor A. Herz of the CERN organization for lending us the emulsion stack used in the present work. We are thankful to the University Grants Commission (U.G.C.) and the Council of Scientific and Industrial Research, India, for providing us with the financial assistance for the project. S. S. thanks U.G.C. for the grant of a fellowship. We are also grateful to J. Bhowmik, S. Goel, and M. Ghosh for careful scanning and valuable technical assistance. Thanks are due to S. K. Kaul for some useful suggestions and to S. K. Jha for help in the computation of some results.

APPENDIX A

The original thicknesses of the pellicles were not recorded before processing. However, in the present experiment, the original thickness for each plate could be estimated from an analysis of ranges of muons from π-μ-e decay events. The total sample of 200 μ tracks in each plate was divided into three subsamples according to their steepness (s), defined as $s = (100 \sum_i |Z_i| / \sum_i \kappa_i)$, where Z_i and κ_i are the vertical and horizontal projections of the ith segment of a μ track. Thus subsamples of tracks having (i) $s \leq 10\%$, (ii) $10\% < s < 20\%$, and (iii) $s \geq 20\%$ were formed for each pellicle. Assuming different values of shrinkage factor, actual ranges of μ tracks were calculated and the mean muon range versus shrinkage factor curves were plotted for the three subsamples of μ tracks in each plate. Figure 15 shows these curves for one of the plates. The projected angles of μ tracks in each pellicle were measured in a period of a few days under steady conditions of temperature and humidity. Therefore, the true muon range and the mean shrinkage factor for the period are given by the point of intersection of these curves. Then using the instantaneous value of the emulsion thickness, its original thickness was calculated, which was used in further calculations of shrinkage factor.

APPENDIX B

To take account of the spurious scattering, it has been the common practice to estimate its magnitude for a given cell length from the measurements on beam tracks. In fact, the spurious scattering varies even with track to track almost randomly with the nature and energy of the secondary particle. Therefore, it seems to be more

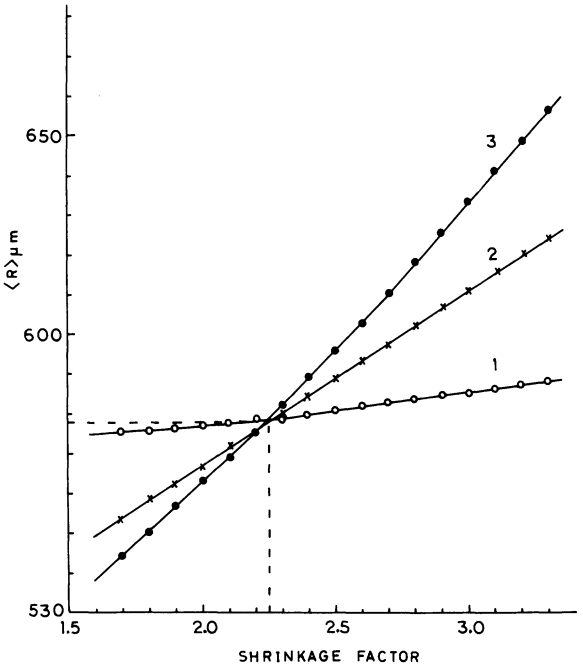

FIG. 15. Plot of mean muon range $\langle R \rangle$ against shrinkage factor for various steepnesses (s), (1) $s \leq 10\%$, (2) $10\% < s < 20\%$, and (3) $s \geq 20\%$.

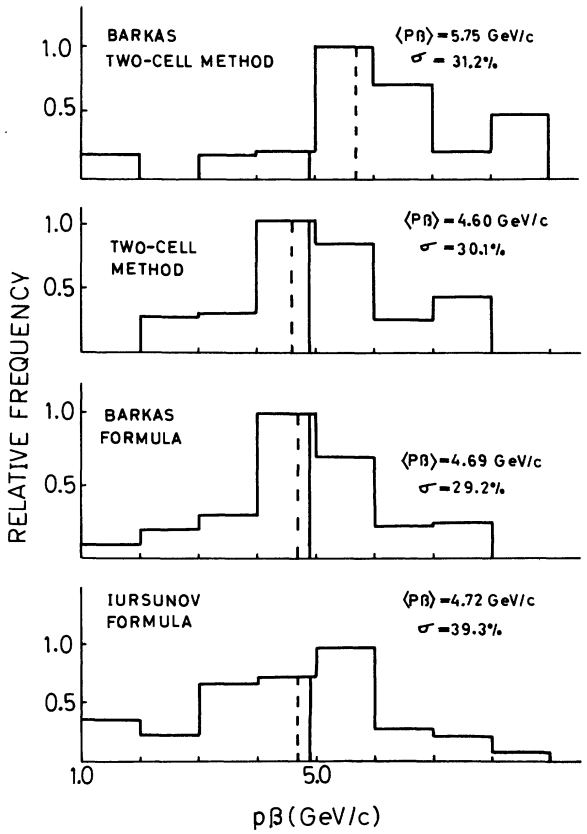

FIG. 16. Distributions of estimates of $p\beta$ by different methods on beam tracks of $p\beta$=4.91 GeV/c, indicated by solid line. The dashed line indicates the mean of the observed distribution.

rational to eliminate the contribution of spurious scattering statistically from the observations on individual tracks. Hence we have made a critical study of the well-known statistical methods of eliminating noise from observations on individual tracks, namely, the Iursunov formula,[30] the ordinary two-cell length method,[31] the Barkas method of two cell lengths,[32] and the Barkas formula.[33]

To test the relative merits of the above four methods, we have applied them to the observations on individual tracks of beam antiprotons having $p\beta = 4.91$ GeV/c. Cell length of 1500 μm was used and scattering measurements were made on only those beam tracks which have length ≥ 4.5 mm per plate. The results for the various methods have been shown in Fig. 16. The Iursunov formula gives the mean value of $p\beta$ closest to the expected one, but its dispersion is the largest; the Barkas method of two cell lengths gives the highest mean and the distribution is generally biased toward the higher values. The Barkas formula and the ordinary two-cell-length method are almost on the same footing. Relatively speaking, the latter is more skewed toward the higher values. Moreover, in this method (and also in the Barkas method of two cell lengths), one requires knowledge of the law of variation of spurious scattering with cell length. For the present case this law was determined from observations on beam tracks and was reemployed in the two-cell-length formulas. This might also improve the agreement of this method with the experiment. Therefore, the Barkas formula is found to be the best statistical method of noise elimination, and hence it was employed to estimate $p\beta$ of the secondary shower tracks.

[1]J. V. Allaby, Yu. B. Bushnin, S. P. Denisov, A. N. Diddens, R. W. Dobinson, S. V. Donskov, G. Giacomelli, Yu. P. Gosin, A. Klovning, A. I. Petrukhin, Yu. D. Prokoshkin, R. S. Shuvalov, C. A. Ståhlbrandt, and D. A. Stoyanova, Phys. Lett. 30B, 500 (1969).

[2]T. Ferbel, A. Firestone, J. Johnson, J. Sandweiss, and H. D. Taft, Nuovo Cimento 38, 12 (1965).

[3]C. Baltay, C. Y. Chien, T. Ferbel, H. L. Kraybill, J. Lach, J. Sandweiss, H. D. Taft, N. Yeh, D. J. Crennell, J. K. Kopp, Y. Oren, D. L. Stonehill, A. M.

Thorndike, and M. Webster, in *Proceedings of the Twelfth International Conference on High Energy Physics, Dubna, 1964,* edited by Ya. A. Smorodinskii *et al.* (Atomizdat, Moscow, 1966).
[4]I. Bar-Nir, A. Brandstetter, S. Dagan, G. Gidal, J. Grunhaus, Y. Oren, J. Schlesinger, and G. Alexander, Nucl. Phys. B20, 45 (1970).
[5]R. Sears, R. Socash, and L. Marshall Libby, Phys. Lett. 29B, 700 (1969).
[6]F. C. Chen, Nuovo Cimento 62A, 113 (1969).
[7]A. G. Frodesen, O. Skjeggestad, R. S. Moore, and S. Reueroft, Nucl. Phys. B10, 307 (1969).
[8]G. Ranft, Nuovo Cimento 58A, 425 (1968).
[9]C. P. Wang, Phys. Lett. 30B, 115 (1969).
[10]K. Böckmann, B. Neller, E. Paul and B. Wagini, I. Borecka, J. Diaz, U. Heeren, U. Liebermeister, E. Lohrmann, E. Raubold, P. Söding, and S. Wolff, J. Kidd, L. Mandelli, L. Mosca, V. Pelosi, S. Ratti, and L. Tallone, Nuovo Cimento 42, 954 (1966).
[11]R. Armenteros and B. French, *High Energy Physics,* edited by E. H. S. Burhop (Academic, New York, 1969), Vol. 4, p. 237.
[12]P. S. Gregory, P. Grossmann, P. Mason, H. Muirhead, S. O. Holmgren, and N. K. Yamdagni, Phys. Lett. 43B, 228 (1973).
[13]I. Raghvan, A. A. Kamal, S. V. Padmavathi, R. Rao, and A. Santhalakshmi, Nuovo Cimento 65, 362 (1970).
[14]W. H. Barkas, *Nuclear Research Emulsions* (Academic, New York, 1963), Vol. 1, p. 70.
[15]R. E. Cavanaugh, D. M. Haskin, and M. Schein, Phys. Rev. 100, 1263 (1955).
[16]S. Biswas, B. Peters, and Rama, Proc. Indian Acad. Sci. 41A, 154 (1955).
[17]C. A. Nicoletta, P. J. McNulty, and P. L. Jain, Phys. Rev. 164, 1693 (1967).
[18]P. H. Fowler and D. H. Perkins, Philos. Mag. (7) 46, 587 (1955).
[19]B. Bhowmik, S. Singh, and S. K. Jha, Nuovo Cimento 3A, 250 (1971).
[20]H. Ezawa, Nuovo Cimento 11, 745 (1959).
[21]B. Edwards, I. Bosty, D. H. Perkins, K. Pinkau, and Y. Reynolds, Philos. Mag. 3, 710 (1958).
[22]R. Rajaraman and R. P. Jain, Phys. Rev. D 4, 2768 (1971).
[23]R. R. Daniel, N. K. Rao, P. K. Malhotra, and Y. Tsuzuki, Nuovo Cimento 16, 1 (1960).
[24]J. Finkelstein and K. Kajantie, Nuovo Cimento 56A, 659 (1968).
[25]G. Bozóki, E. Gombozi, M. Posch, and L. Vanicsek, Nuovo Cimento 44A, 881 (1969).
[26]Z. Koba and S. Takagi, Nuovo Cimento 10, 755 (1958).
[27]W. L. Kraushaar and L. J. Marks, Phys. Rev. 93, 326 (1954).
[28]G. Cocconi, L. J. Koestler, and D. H. Perkins, Lawrence Radiation Laboratory Report No. UCID-1444, 1961 (unpublished).
[29]E. M. Friedländer, Nuovo Cimento 41, 417 (1966).
[30]K. A. Iursunov, I. Ya Charnikov, and K. V. Sharapov, in Proceedings of the Third International Conference on Nuclear Photography, Moscow, 1960.
[31]C. F. Powell, P. H. Fowler, and D. H. Perkins, *The Study of Elementary Particles by the Photographic Method* (Pergamon, New York, 1959), p. 122.
[32]Page 314 of Ref. 14.
[33]Page 313 of Ref. 14.